metals

MDPI

Article

Quenching and Partitioning of Multiphase Aluminum-Added Steels

Tuomo Nyyssönen [1,2,*], Olli Oja [3], Petri Jussila [3], Ari Saastamoinen [1], Mahesh Somani [4] and Pasi Peura [1]

1 Laboratory of Metals Technology, Faculty of Engineering and Natural Sciences, Materials Science, Tampere University, Korkeakoulunkatu 6, 33720 Tampere, Finland; ari.saastamoinen@tuni.fi (A.S.); pasi.peura@tuni.fi (P.P.)
2 Outotec Oyj, Pori Outotec Research Center, Kuparitie 10, 28330 Pori, Finland
3 Product Development, SSAB Europe Oy, Harvialantie 420, 13300 Hämeenlinna, Finland; olli.oja@ssab.com (O.O.); petri.jussila@ssab.com (P.J.)
4 Faculty of Technology, Materials and Mechanical Engineering, University of Oulu, 90014 Oulun Yliopisto, Finland; mahesh.somani@oulu.fi
* Correspondence: tuomo.nyyssonen@outotec.com or tuomo.nyyssonen@tut.fi; Tel.: +358-503-721-641

Received: 27 February 2019; Accepted: 19 March 2019; Published: 22 March 2019

Abstract: The quenching and partitioning response following intercritical annealing was investigated for three lean TRIP-type high-Al steel compositions. Depending on the intercritical austenite fraction following annealing, the steels assumed either a ferrite/martensite/retained austenite microstructure or a multiphase structure with ferritic, bainitic and martensitic constituents along with retained austenite. The amount of retained austenite was found to correlate with the initial quench temperature and, depending on the intercritical annealing condition prior to initial quenching, with the uniform and ultimate elongations measured in tensile testing.

Keywords: steel; martensite; austenite; quenching; partitioning; dilatometry

1. Introduction

Intercritical annealing of low-alloy steel occurs in the temperature regime between the *Ac1* and *Ac3* temperatures, where thermodynamic equilibrium corresponds to some mixture of the austenite and ferrite phases. The amount of austenite at the conclusion of intercritical annealing depends on several factors, such as the starting microstructure, heating rate [1] and, more importantly, the alloying contents of the steel. Upon quenching at higher than critical cooling rates, the intercritical austenite phase is transformed to martensite, resulting in low-alloy dual-phase steel consisting of martensitic islands in a matrix of ferritic grains.

If the quenching is interrupted somewhere between the martensite start temperature M_s and the temperature where the last of the austenite transforms (M_f), the martensitic transformation will be incomplete and the martensitic islands will include some untransformed metastable austenite. If the steel is then transitioned for a certain duration to a suitable intermediate holding temperature (also commonly referred as 'partitioning temperature'), this metastable austenite can be either partially or fully stabilized down to room temperature by enriching it with carbon partitioned from the carbon-supersaturated martensite. The resulting microstructure then would consist of martensitic islands interspersed with carbon-enriched retained austenite, suspended in the ferritic matrix. In effect, the intercritical austenite phase has undergone a heat treatment known as quenching and partitioning (Q&P), originally proposed in 2003 by Speer et al. [2].

The end goal of the Q&P treatment of intercritical austenite is to improve the ductility of a dual-phase microstructure via the strain-induced transformation of the retained austenite to martensite

during deformation, essentially increasing the strain hardening capability of the steel. It was found by some of the present authors in a previous study [3] that austenite stabilized in this manner can increase ductility even for a low-carbon, high-aluminum steel. However, it was recently observed by Tan et al. [4] that the ability of the retained austenite to contribute to strain hardening depends on its localization, morphology and stability essentially with respect to the carbon-content. They found that if the deformation occurs primarily in the ferrite phase, the transformation of retained austenite to martensite remains limited, thus limiting the total elongation. A fine film-like morphology (resulting in high mechanical stability) and localization of the austenite away from ferrite-prior austenite interfaces will also promote this type of undesirable mechanical stability.

Successfully promoting quenching and partitioning in a steel imposes some requirements on alloying. First, the steel must have the ability to suppress or delay the formation of carbides or other precipitates during partitioning. This is typically achieved by adding a combination of ferrite-stabilizing elements such as aluminum [5], silicon [6] or chromium [7]. Second, the steel must contain a sufficient amount of carbon to enable stabilizing an optimum retained austenite fraction to achieve the desired increase in ductility. Third, the steel must be sufficiently hardenable in order to reach the initial quench temperature without allowing undesired ferritic or bainitic phase transformations during the initial cooling step.

Intercritical annealing opens up some interesting possibilities for controlling the condition of the austenite at the conclusion of annealing. The grain size and the relative fraction of the intercritical austenite can be controlled to a large extent by suitably varying the annealing parameters [1,8,9]. The growth of the austenite phase in low- and medium-carbon steels has been observed in various research works to be controlled essentially by the diffusion of carbon across the interphase boundary. Therefore, carbon can be expected to partition nearly completely to austenite [1,10], while the partitioning of heavier elements (such as silicon, aluminum or manganese) is usually limited and will depend on the annealing temperature and duration [11].

The conditioning of the austenite will drastically affect the quenching response, both in terms of martensite start temperature M_s as well as the hardenability. Assuming total partitioning of carbon from ferrite to austenite, a smaller initial fraction of austenite will greatly increase its carbon content. This will both decrease M_s and improve hardenability [12], at least up to the eutectoid composition. To illustrate the point further, three preliminary calculations were made with the thermodynamic and kinetic calculation software JMATPRO® [13] for two of the experimental steels studied in this work: Steel A and Steel B (see Table 1 for chemical composition). JMATPRO was used to calculate continuous cooling transformation (CCT) curves based on the model by Kirkaldy et al. [14] modified by Lee and Bhadeshia [15]. Figure 1 shows the CCT curves for the steels with modified carbon contents, from nominal composition to carbon contents corresponding to 50 and 25 vol % fraction of intercritical austenite at the conclusion of annealing (assuming full partitioning of carbon). In the figure, the 50 vol % fraction of austenite is indicated by an assumed carbon content of 0.32C for Steel A and 0.22C for Steel B, and 25 vol % austenite content is indicated by 0.64C for Steel A and 0.44C for Steel B. Dashed lines in the figure indicate continuous cooling curves corresponding to a linear cooling rate of 10 °C/s, which is a realistically achievable cooling rate in modern continuous annealing lines. Referring to Figure 1, the onset of bainite transformation is delayed due to an increase in carbon content at lower austenite fractions. At an austenite fraction of 25 vol %, bainite transformation is avoided completely at a cooling rate of 10 °C/s, based on the JMATPRO® calculations.

Table 1. Compositions of the experimental steel grades.

wt %	C	Mn	Al	Ni	Ti + Nb + V	Si + Cr + Mo	Balance
Steel A	0.16	2.08	1.03	0.044	0.008	0.689	Fe and traces of Cu, P, S
Steel B	0.11	2.65	0.81	0.041	0.035	0.978	Fe and traces of Cu, P, S
Steel C	0.16	1.62	1.31	0.041	0.023	0.498	Fe and traces of Cu, P, S

These calculations do not take into account prior austenite grain size, which has been observed to have a significant effect on the martensite transformation of intercritically annealed steel in a previous study [8]. Essentially, the prior austenite grain size potentially remains very small during intercritical annealing, further reducing the M_s temperature. Such an effect of fine austenite grain size on M_s has been exhaustively investigated, for instance, by Yang and Bhadeshia [16].

Austenite conditioning via intercritical annealing was shown to affect the quenching and partitioning response of a high-aluminum steel in a previous study [3]. In this case, the prior austenite grain size was of the order of 1.5 µm and the austenite had a high carbon content directly after intercritical annealing. This decreased M_s significantly beyond the value predicted by empirical equations and promoted the formation of martensite with a small packet size and coarse, irregularly-shaped lath morphology. This, in turn, resulted in blocky rather than film-like retained austenite formation, situated primarily at prior austenite and packet boundaries. The amount of retained austenite was found to correlate well with the initial quench temperature, as well as the uniform and ultimate elongations of the studied steels. The effect of intercritical annealing on M_s was also observed by Yi et al. [17], who showed that with a suitably high carbon and aluminum content in the steel, intercritical annealing can be used to lower the initial quench temperature *QT* to ambient temperature or lower. Q&P-aided dual-phase microstructures were also produced for a Fe-0.2C-2.0Mn-1.5Si (wt %) steel after intercritical annealing by Wang et al. [18].

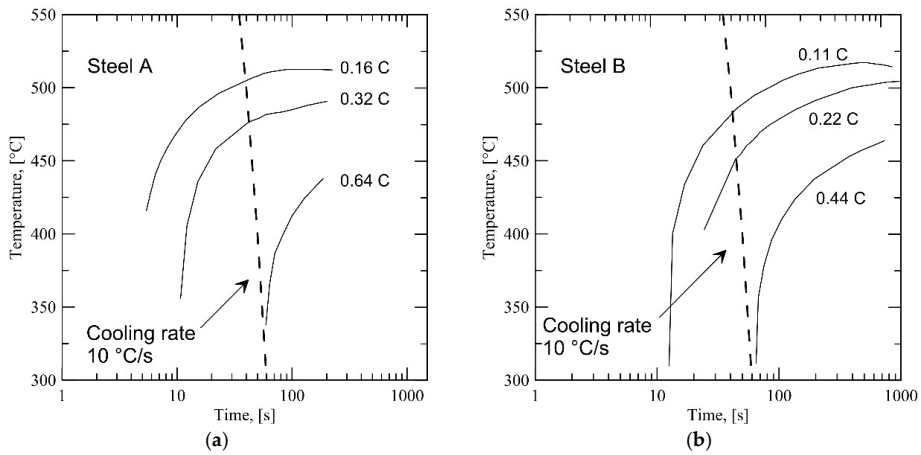

Figure 1. Partial CCT (continuous cooling transformation) curves showing the bainite start lines, calculated for (**a**) Steel A and (**b**) Steel B (see Table 1 for compositions), assuming full partitioning of carbon from ferrite to austenite during intercritical annealing. The carbon concentration for each annealing condition is indicated in wt % next to the corresponding bainite start line.

The above discussion should emphasize the point that the condition of the austenite at the conclusion of intercritical annealing should be known (at least at the level of prior austenite grain size and its carbon content), if any reliable estimation for Q&P heat treatment parameters should be made beforehand. Otherwise, it is necessary to determine M_s experimentally by suitable methods, such as dilatometry.

Despite several promising early results [3,4,17,18], the alloy compositions that have been investigated thus far are challenging to produce in an industrial setting with the current level of knowledge and technology. Furthermore, either the high silicon content of the steels makes hot dip galvanizing difficult [19] or the high aluminum or other alloying contents complicate the casting procedure.

With this in mind, the quenching and partitioning response was investigated for three experimental alloys following intercritical annealing: a conventional aluminum-alloyed TRIP-type steel and two novel lean-alloyed complex phase-type compositions with a mixture of aluminum, silicon and chromium elements as suppressors of carbide formation. The steels have been cast,

rolled and could be hot dip galvanized in an industrial setting, at the current level of technology. The annealing temperatures and timeframes investigated here were also selected from the viewpoint of industrial relevance.

The phase transformation behavior during quenching of the steels was investigated via dilatometry and suitable quenching and partitioning parameters were determined based on the results. The effect of quench temperature on the retained austenite content and the morphology of the various phases in the final microstructures were investigated via optical microscopy, X-ray diffraction (XRD) and electron backscatter diffraction (EBSD). Preliminary evaluation of Q&P treated samples was made in respect of tensile properties.

2. Materials and Methods

The compositions of the investigated steels are shown in Table 1. The steels were supplied in a cold rolled, fully hard condition as 1.3-mm thick sheets.

Dilatometry experiments were conducted with a Gleeble 3800 thermomechanical simulator (Dynamic Systems Inc., Poestenkill, NY, USA) to determine the M_s temperatures of the steels after intercritical annealing. 10 mm × 60 mm specimens were cut from the sheets for the experiments. The specimens were subjected to a computer-controlled resistance heating followed by controlled cooling, with the aid of compressed argon gas below 400 °C down to room temperature. The temperature of each specimen was monitored with a K-type thermocouple, and the dilatation was measured in the transverse direction of the specimen at the thermocouple location using an extensometer fitted with quartz rods. The heat treatment parameters are shown in Table 2.

Table 2. Dilatometry parameters for the steels. *HR* = heating rate, *HT* = time at annealing temperature, *AT* = annealing temperature and *CR* = cooling rate.

HR (°C/s)	*HT* (min)	*AT* (°C)	*CR* (°C/s)
4	3	850	25

The transformation curves were extracted from the dilatometric data by line fitting over the linear thermal contraction portion of both the austenite and martensite phases. Martensite and austenite cooling contraction curves were extrapolated from the linear portions of the curve. The extent of the martensitic transformation was calculated by using the lever rule. A curve was fitted to this data corresponding to the Koistinen-Marburger [20] equation:

$$V_m = 1 - e^{-K(Ms-T)} \quad (1)$$

The martensite start temperature M_s and empirical fitting constant K were determined by curve fitting of Equation (1), using Trust-Region-Reflective Least Squares Algorithm in the Matlab® Curve Fitting Toolbox in Matlab® R2018b (Mathworks Inc., Natick, MA, USA). The transformation data up to a martensite fraction of 0.2 were excluded from the fitting, in order to minimize the effect of initial gradual martensite start on the fit. Two additional fits were also made, excluding data up to 0.4 and 0.6 martensite fraction. Of these three fits, the best fit according to the adjusted R-square statistics, when compared to the whole transformation data, was chosen as the optimum fitting solution. The M_s temperature was obtained directly from the fitting parameters for Equation (1). The fitting procedure is shown schematically in Figure 2.

The specimens were then sectioned in the transverse direction at the thermocouple location and mounted into cold setting resin for metallography. The specimens were ground and polished with colloidal silica Buehler Mastermet2 used in the final polishing step. The specimens were then treated with the color etching procedure proposed by LePera [21]. The polished and etched specimens were examined and micrographed with the Alicona InfiniteFocus G5 profilometer (Optimax IIM Ltd., Market Harborough, UK).

Typical quenching and partitioning parameters were designed for the steels based on the M_s values measured in the dilatometry experiments and the fitted martensitic transformation behavior, Figure 2. The parameters are shown in Table 3. Figure 3 shows a schematic diagram of the Q&P treatment cycle including linear heating and cooling rates.

Heat treatment specimens of 10 mm × 60 mm size were cut from the steel sheets. The Q&P treatments were conducted in the Gleeble 3800 simulator with the pocket jaw grips set at a free span distance of 35 mm. Two specimens were heat treated for each Q&P cycle: one specimen was later used for tensile testing and another for microstructural evaluation and retained austenite measurements using XRD. The test setup was essentially similar to the one employed in dilatometry, with the only difference that the extensometer was not used, if deemed unnecessary.

To determine if significant heating or cooling gradients exist in the specimens during the heat treatment cycles and to assess uniform temperature zone, three thermocouples were fitted on one of the Steel C specimens: one at the center, one 3 mm from center to the side and one 6 mm from center to the other side. It was found that at a distance of 3–6 mm from the controlling thermocouple, the temperature gradient remains below 3–5 °C at all stages of the heat treatment.

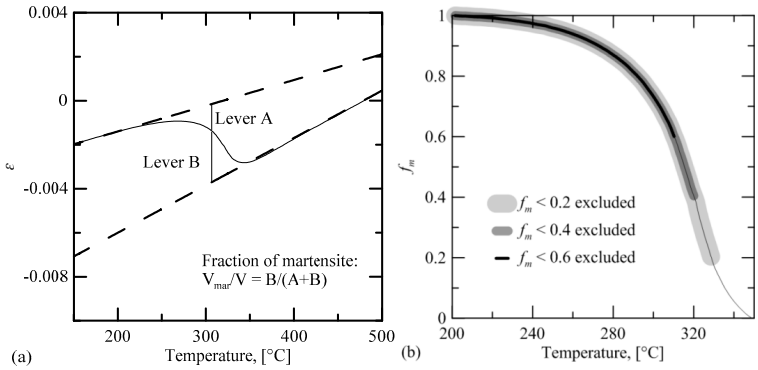

Figure 2. (**a**) The cooling contraction curve around the martensitic transformation. (**b**) The martensite volume fraction with respect to temperature extrapolated from the data shown in (**a**).

The retained austenite contents of the Q&P specimens were measured at room temperature using X-ray diffraction. A thickness of ~0.2 mm was ground from the specimen surface using a P800 SiC emery paper. The specimens were then ground with progressively finer papers, ending with the roughness P2000 in accord with standard polishing practice. The specimens were then electrolytically polished for 12 s at 40 V with the A2 electrolyte in a Lectropol-5 polisher (Struers Inc., Cleveland, OH, USA). The XRD analyses were conducted with the Panalytical Empyrean X-Ray diffractometer (Malvern Panalytical Ltd., Malvern, UK) using Co K_α-radiation ($40° < 2\theta < 102°$, 40 kV, 45 mA). The site of the thermocouple location was used for centering the X-ray beam on the specimens. The peaks used in the analysis were (110), (200), (211) and (220) for martensite and (111), (200), (220) and (311) for austenite. The method for retained austenite calculation was the four-peak method described in SP-453 [22] (four peaks for both ferrite and austenite). The carbon content was estimated from the measured average austenite lattice parameter using Equation (2) [23]:

$$C_\gamma = (a_\gamma - 0.3555)/0.0044 \quad (2)$$

in which a_γ stands for the average austenite lattice parameter in Å.

After the XRD measurements, the specimens were sectioned in the transverse direction at the location of the thermocouple and prepared for electron backscatter diffraction (EBSD). The specimens were polished in a manner similar to the practice adopted for dilatometry specimens prepared for light optical microscopy. However, the specimens were not etched after polishing. The polished specimens were removed from the mounts, washed in ethanol and placed in a low pressure desiccator overnight

to remove moisture. Prior to electron microscopy, the specimens were cleaned in an evacuated chamber fed with ionized oxygen plasma to remove any leftover organic residues on the surface.

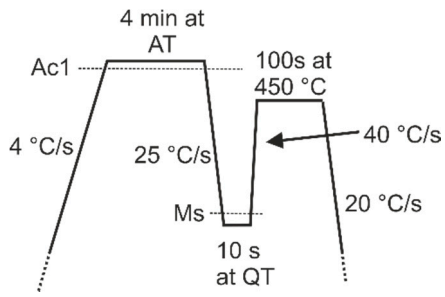

Figure 3. Schematic of the heat treatment cycle for the quenched and partitioned specimens.

Table 3. Annealing temperature (*AT*), initial quench temperature (*QT*), partitioning temperature (*PT*) and holding time at partitioning temperature (t_H) for the heat treated specimens.

Alloy	*AT* (°C)	*QT* (°C)	*PT* (°C)	t_H (s)
Steel A	850	125	450	100
-	-	150	-	-
-	-	175	-	-
Steel B	850	200	450	100
-	-	250	-	-
-	-	275	-	-
-	-	300	-	-
Steel C	850	75	450	100
-	-	100	-	-

The specimens were then subjected to electron backscatter diffraction (EBSD) studies. The scanning electron microscope (SEM) used was a Zeiss ULTRAPLUS UHR FEG-SEM system (ZEISS International, Oberkochen, Germany) fitted with a field emission gun (FEG) and an HKL Premium-F Channel EBSD system with a Nordlys F400 detector (Oxford Instruments plc, Abingdon, UK), which was used for phase contrast and orientation mapping. The parameters for EBSD analysis were 20 kV acceleration voltage, 14 mm working distance and a tilt angle of 70° with a step size of 0.05 µm.

Tensile testing was carried out using an Instron 8800 servohydraulic materials testing machine (Instron, Norwood, MA, USA). Non-standard tensile specimens were prepared by precision milling a 6 mm long, 3.5 mm wide gage area with 1 mm roundings into the center of each specimen. A cooling lubricant jet was used to reduce thermal effects on the specimen during milling. Each specimen was tested in tension to fracture at an engineering strain rate of 0.001 s^{-1}. Elongation was measured using a miniature axial extensometer. The total elongation A was recalculated to correspond to standard test geometry of a 120 mm × 20 mm gage section using the Oliver equation as implemented by ISO 2566/1 [24]:

$$A_2 = A_1 \times \left(\frac{k_1}{k_2}\right)^n \tag{3}$$

where A_2 is the calculated elongation value, A_1 is the known elongation value, k_1 and k_2 are the proportionality ratios of the two test pieces, and n is a material dependent constant. The standard adopts n = 0.4. The proportionality ratios k_1 and k_2 were calculated with the equation:

$$k_1 = \frac{w_s}{\sqrt{w_a t_a}} \tag{4a}$$

$$k_2 = \frac{l_s}{\sqrt{w_s t_a}} \tag{4b}$$

where w_s and l_s are the new width and length, respectively, and w_a, l_a and t_a are the measured width, length and thickness, respectively.

3. Results

3.1. Dilatometry Experiments

Table 4 shows the measured M_s temperatures for the steels estimated from dilatation curves based on dilatometer data. Figure 4 shows examples of the optical micrographs taken from the quenched dilatometry specimens. For Steel A and Steel C, the microstructures consist of martensite (including prior austenite) (lighter shade) and intercritical ferrite (darker shade). For Steel B, Le Pera etching produced an unexpected coloring result: the microstructure appears to consist of a primarily martensitic matrix (brown) with islands of intercritical ferrite (white).

Assuming that no ferrite transformation occurred during quenching, the intercritical austenite fraction can be estimated from the amount of the lighter phase (martensite) in the optical micrographs by image analysis [21]. The intercritical austenite contents could be estimated from the micrographs for Steel A and Steel C and they are shown in Table 4. In Steel B, the amount of intercritical austenite was judged to be approximately 65 vol %, although a reliable analysis is not possible due to the poor etching response. Assuming full partitioning of carbon, 65 vol % of austenite would correspond to an M_s temperature of 339 °C when calculated with the method proposed by Bhadeshia [25,26], which is in line with the measured M_s value shown in Table 4.

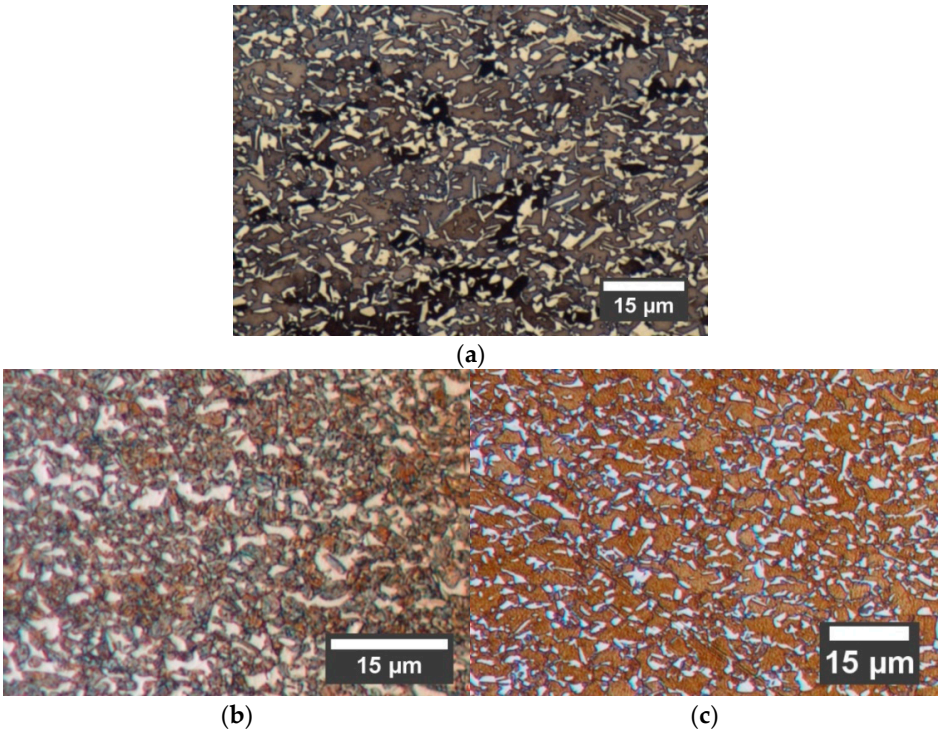

Figure 4. Typical examples of the optical micrographs of the dilatometry specimens for (**a**) Steel A, (**b**) Steel B and (**c**) Steel C.

Table 4. Experimentally determined M_s temperatures.

Alloy	AT (°C)	M_s (°C)	γ_{frac} (vol %)
Steel A	850	203	27 ± 1
Steel B	850	339	~65 (see text)
Steel C	850	116	23 ± 0.5

3.2. Q&P Experiments, Steel A

Figure 5 shows examples of the obtained XRD spectra for the quenched and partitioned specimens. There is clearly an appreciable amount of retained austenite following quenching and partitioning. The peaks corresponding to the ferrite phase coincide almost exactly among Steels A, B and C, while a slight scatter in the locations of the austenite peaks can be detected between the Steels. This is an indication that the lattice parameters of austenite in the Steels are affected by carbon partitioned from supersaturated martensite, each Steel having received a different amount of carbon in the austenite phase after quenching to the temperatures indicated in the figure.

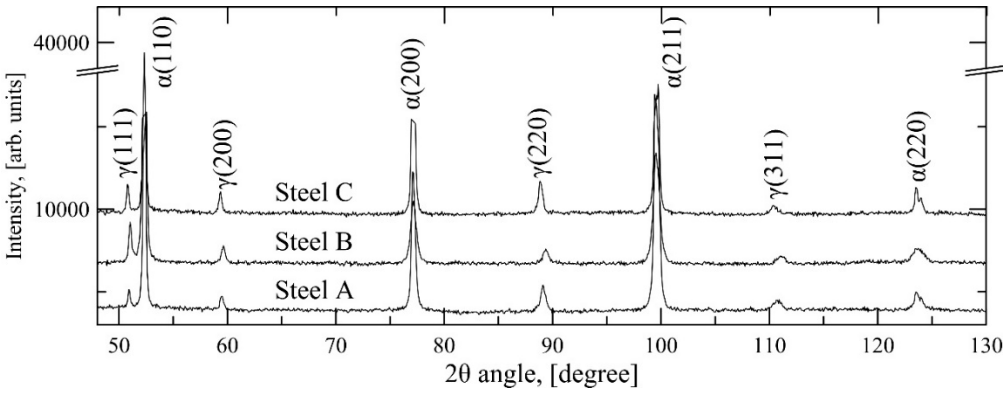

Figure 5. The observed XRD spectra for Steel A, quenched to 175 °C, Steel B, quenched to 300 °C and Steel C, quenched to 100 °C. All specimens were annealed at 850 °C for 4 min and partitioned at 450 °C for 100 s.

Figure 6 shows the measured retained austenite fraction and the calculated austenite carbon content with respect to the initial quench temperature for Steel A. As can be seen from the figure, the quench temperature correlates with the amount of retained austenite in the final microstructure. The carbon content of the retained austenite drops as the initial quench temperature is raised.

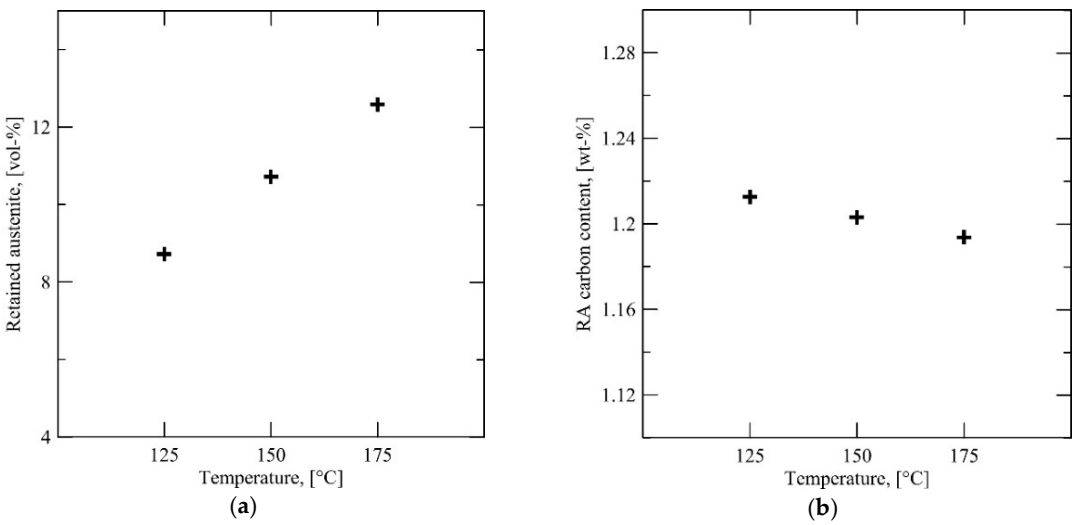

Figure 6. (**a**) The retained austenite fraction of Steel A with respect to initial quench temperature *QT*. (**b**) The carbon content of the retained austenite with respect to *QT*. Specimens annealed at 850 °C, quenched to *QT* and partitioned at 450 °C for 100 s.

Figure 7 shows the measured 0.5% proof strength (denoted R_{p05} in the Figures), ultimate tensile strength R_m, uniform elongation Ag and the total elongation A with respect to the initial quench

temperature. Figure 6b shows that *Ag* correlates with the initial quench temperature. There is a slight inverse correlation with the total elongation. It is to be noted that the R_m practically stays at about 1000 MP irrespective of the quench temperature.

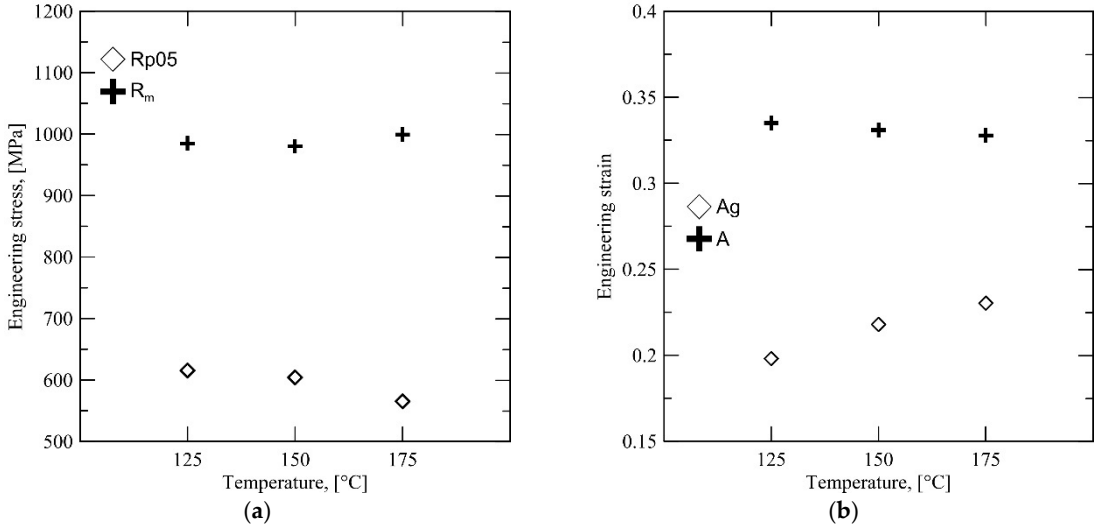

Figure 7. (**a**) The measured 0.5% proof strength and R_m values for Steel A with respect to *QT*. (**b**) The uniform elongation *Ag* and total elongation *A* for Steel A with respect to *QT*. Specimens annealed at 850 °C, quenched to *QT* and partitioned at 450 °C for 100 s.

3.3. Q&P Experiments, Steel B

Figures 8 and 9 show the results of the XRD measurements and tensile tests for Steel B similar to Figures 6 and 7. The behavior of Steel B differs from Steel A. Instead of a steady reduction in austenite fraction, there is an initially high amount (12 vol %) at *QT* = 300 °C followed by an appreciable drop at *QT* = 275 °C to a nearly stable austenite fraction (7–8 vol %) irrespective of further reduction in *QT* temperature down to 200 °C, Figure 8a. The corresponding average carbon content in retained austenite decreased from about 1.2% to 1% with an increase in *QT* from 200 to 300 °C, Figure 8b.

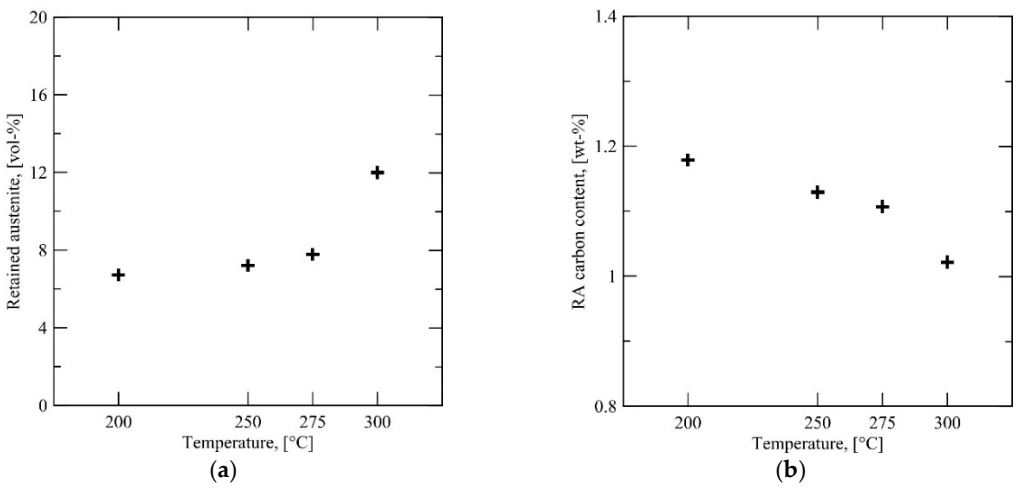

Figure 8. (**a**) The retained austenite fraction of Steel B with respect to initial quench temperature *QT*. (**b**) The carbon content of the retained austenite with respect to *QT*. Specimens annealed at 850 °C, quenched to *QT* and partitioned at 450 °C for 100 s.

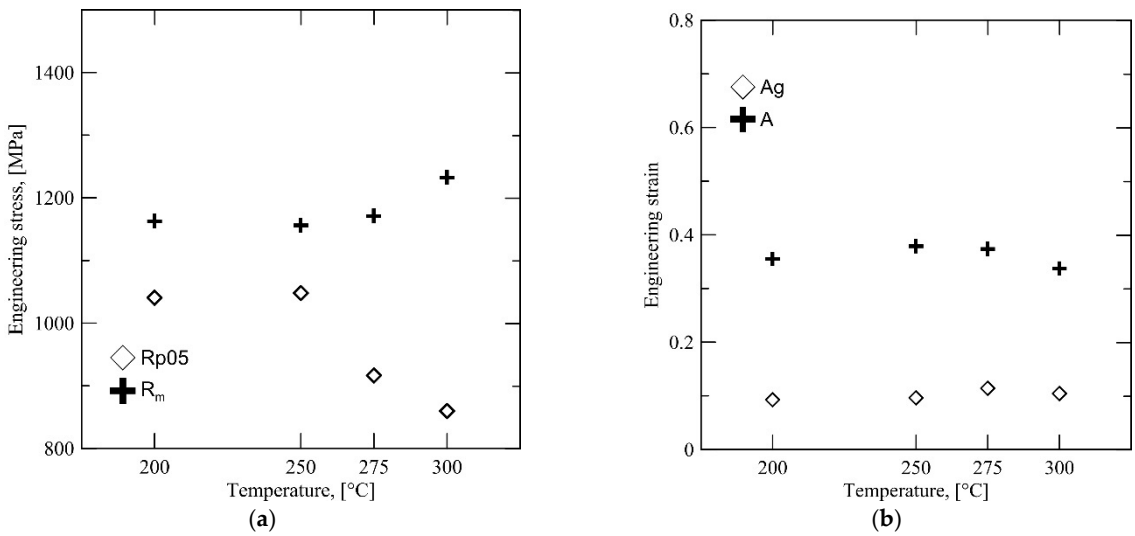

Figure 9. (**a**) The measured 0.5% proof strength and R_m values for Steel B with respect to *QT*. (**b**) The uniform elongation *Ag* and total elongation *A* for Steel B with respect to *QT*. Specimens annealed at 850 °C, quenched to *QT* and partitioned at 450 °C for 100 s.

Figure 9 shows the results of the tensile property characterization of the Steel B specimens. Interestingly, there is a significant drop in yield strength beyond the *QT* > 250 °C. The low yield strength at *QT* = 300 °C is, however, accompanied by a high R_m of 1250 MPa, even though the *Ag* and total elongation *A* seem somewhat insensitive to the *QT*.

3.4. Q&P Experiments, Steel C

The XRD measurements and tensile test results for Steel C are shown in Figures 10 and 11. The behavior of Steel C is very similar to Steel A, as the retained austenite fraction drops with decreasing *QT*. The higher retained austenite fraction of ≈11 vol % at *QT* = 100 °C corresponds to a significant increase in both uniform and total elongations, as well as a drop in yield strength.

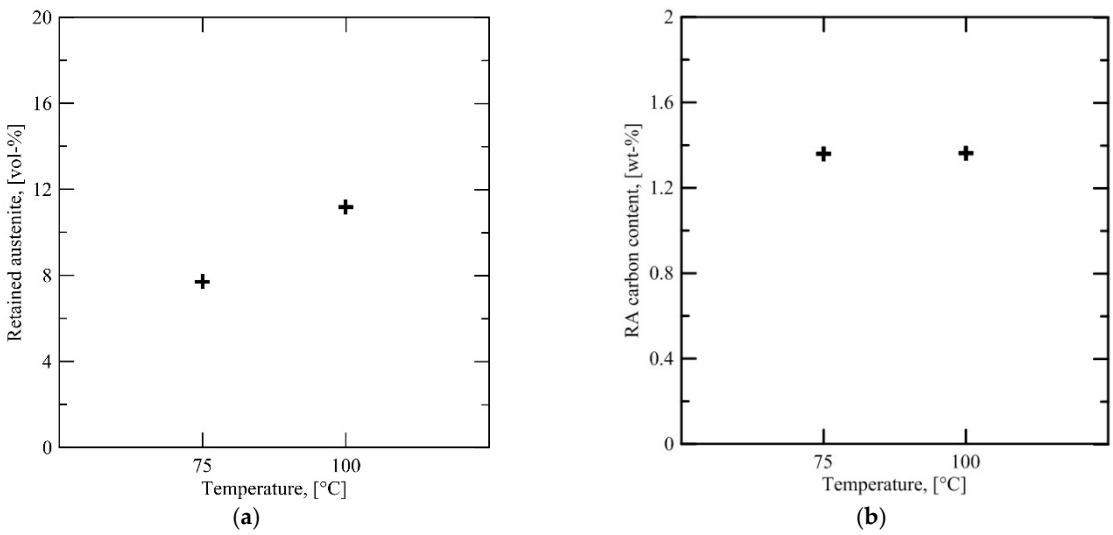

Figure 10. (**a**) The retained austenite fraction of Steel C with respect to initial quench temperature *QT*. (**b**) The carbon content of the retained austenite with respect to *QT*. Specimens annealed at 850 °C, quenched to *QT* and partitioned at 450 °C for 100 s.

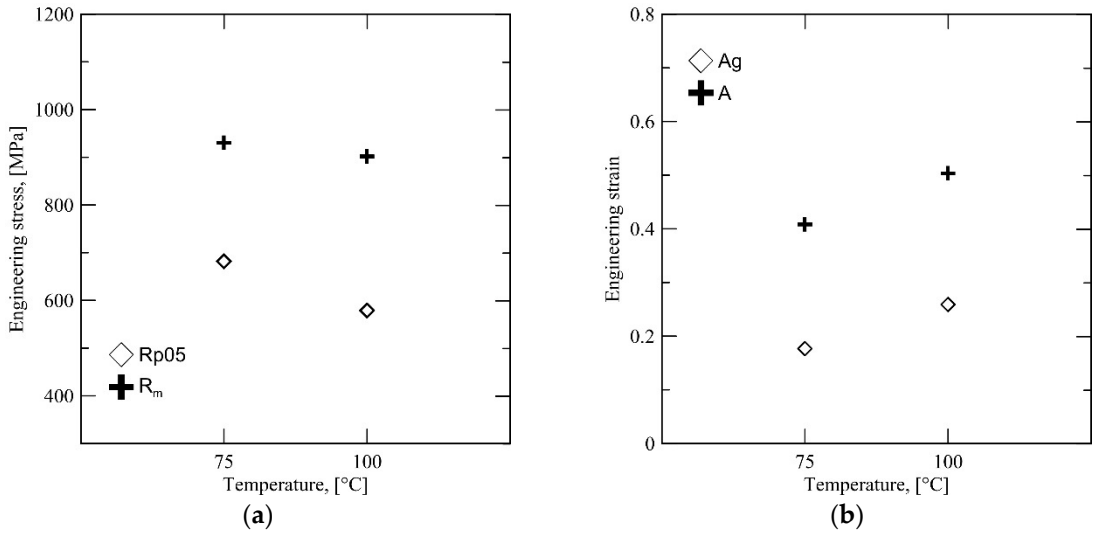

Figure 11. (**a**) R_{p05} and R_m and (**b**) uniform and total elongations for Steel C with respect to initial quench temperature *QT*. Specimens annealed at 850 °C, quenched to *QT* and partitioned at 450 °C for 100 s.

3.5. EBSD Measurements

Figure 12 shows representative results of the EBSD measurements as band contrast maps overlaid with austenite grains (shown in random coloring). Prior austenite and packet boundaries were determined using a previously developed iterative reconstruction algorithm [8,27] and are shown in red (packet boundaries) and black (prior austenite grain (PAG) boundaries and ferrite boundaries).

The observed microstructures in Figure 12a,c show that the martensitic transformation has been heterogeneous on a grain-by-grain basis for Steels A and C: untransformed, partially transformed and almost completely transformed austenite grains can be found in the microstructure. It should be noted that some austenite has probably transformed to martensite during EBSD specimen preparation, as the austenite fraction in EBSD measurements was much lower than in XRD.

Steel B does not exhibit a typical martensitic lath structure, although crystallographic analysis with the iterative method shows the presence of block- and packet-type subunits within prior austenite grains. This is an indication that some degree of bainite transformation has taken place either during the initial quenching or the partitioning stage of the heat treatment. In addition, several large, irregular-shaped intercritical ferrite grains are present in the microstructure.

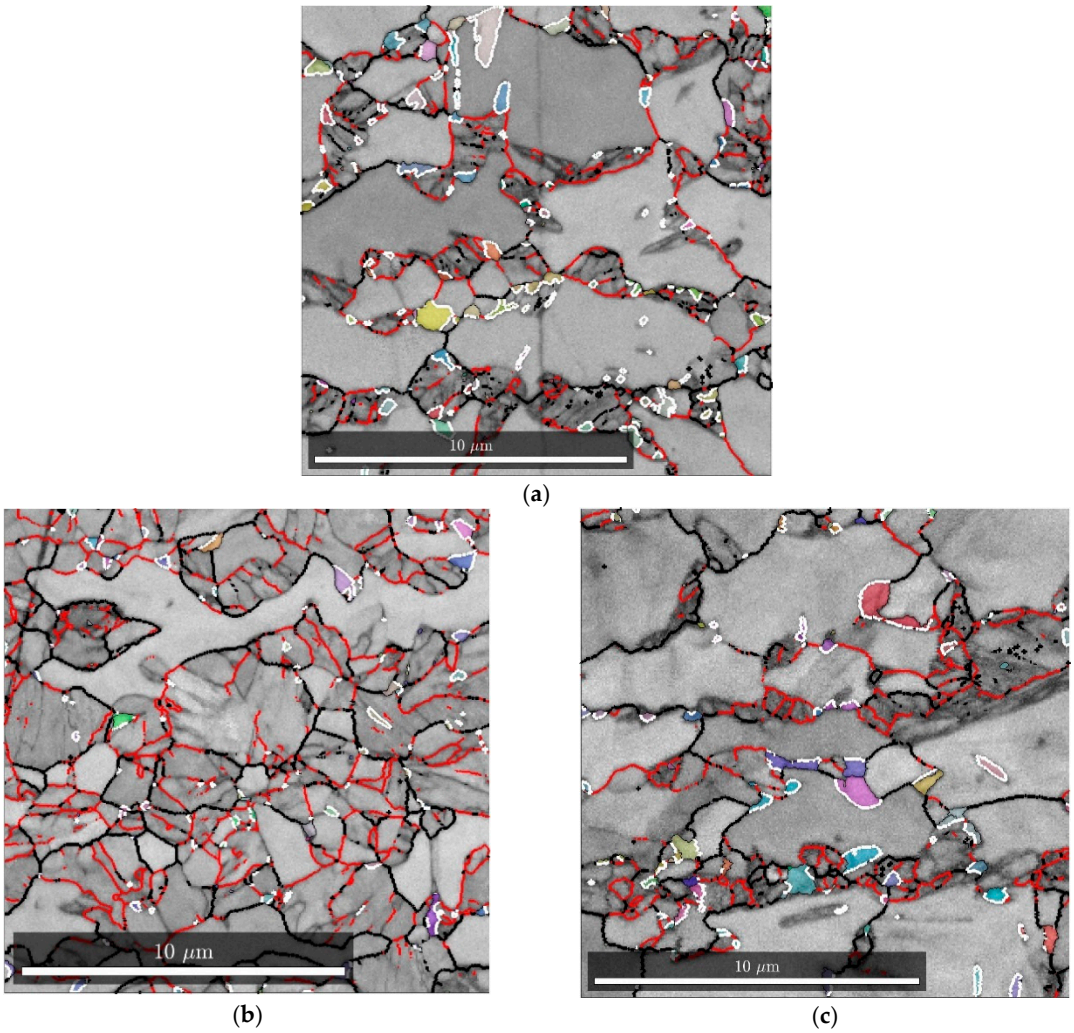

Figure 12. Electron backscatter diffraction (EBSD) band contrast image overlaid with indexed retained austenite grains (random coloring). White boundaries indicate Kurdjumov–Sachs type relationship between γ and α. Black boundaries mark prior austenite grains and red boundaries indicate packet boundaries. (**a**) Steel A quenched to 150 °C, (**b**) Steel B quenched to 275 °C and (**c**) Steel C quenched to 100 °C. All specimens partitioned at 450 °C for 100 s.

4. Discussion

Based on the image analysis of the dilatometry specimens, there is an approximately 27 vol % intercritical austenite fraction in the microstructure of the Steel A after annealing. Assuming that all of the untransformed austenite that remains directly after the interrupted quenching is stabilized with carbon and is also retained at room temperature; 55 vol % is transformed at 175 °C, 63 vol % at 150 °C and 70 vol % at 125 °C. Fitting the Koistinen-Marburger equation to these values does not give a meaningful result, because the apparent martensitic transformation is too gradual with respect to temperature to obtain a good fit. Besides, martensite finish temperature M_f is an indistinct term. It is therefore probable that the martensitic transformation is not actually homogeneous in the microstructure and the degree of transformation varies from grain to grain. This conclusion is supported by the EBSD maps in Figure 11a, which shows a heterogenous martensitic transformation. The behavior of Steel C appears to follow a similar trend, based on the image analysis, XRD and EBSD results.

The behavior of Steel B differs from that of Steels A and C. Instead of a steady reduction in austenite fraction, there is an initially high amount at QT = 300 °C followed by an appreciable drop at QT = 275 °C to a nearly stable austenite fraction irrespective of further QT temperature reduction.

As shown by Figure 4b, there is much more austenite in the microstructure of Steel B after intercritical annealing compared to Steels A and C. This has two consequences—the average carbon content of the austenite is significantly lower (assuming total partitioning of carbon) and austenite grain size is higher. Both factors lower the critical driving force necessary for martensite nucleation, contributing to the rapid formation of martensite when lowering QT past 300 °C. It is possible that autocatalytic nucleation ("burst martensite" [28]) accelerates the rate of transformation. The rapid martensite formation is shown in Figure 13, which displays the retained austenite content with respect to QT overlaid with the dilatation curve in the temperature regime of the martensitic transformation.

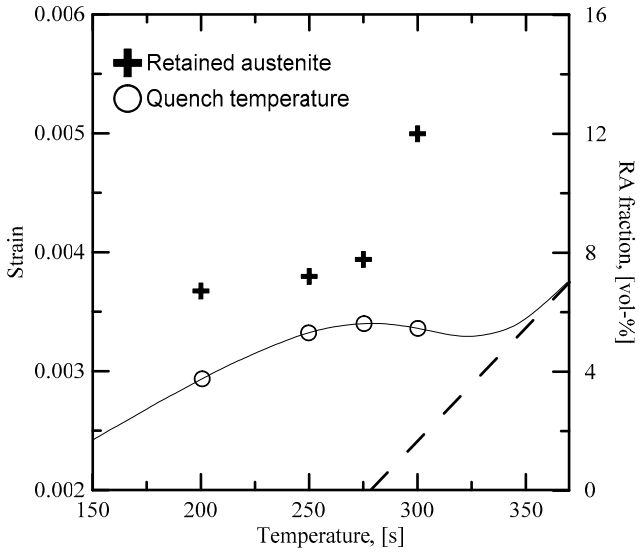

Figure 13. The dilatation curve of Steel B in the regime of martensite transformation, with the retained austenite content with respect to the initial quench temperature QT on the secondary y-axis.

Interestingly, the uniform elongation Ag does not correlate with the high retained austenite content at 300 °C. Instead, there is a significant drop in yield strength, accompanied with a significant rise in R_m, as shown by Figure 9. This behavior is likely to be caused by a combination of both high retained austenite fraction and the effect of the different austenite morphology characteristic to this QT. Figure 8b shows that the average carbon content of the austenite phase after quenching to 300 °C is lower, which should also affect mechanical stability. The presence of unstable austenite grains results in a very high degree of strain hardening at the initial stages of deformation and consequently results in a high R_m combined with a low initial yield point. The unstable austenite grains are unable to contribute to ductility during later stages of deformation, having been completely transformed at an earlier stage and resulting in a lower total elongation A, as shown by Figure 9b.

From a microstructure point of view, the expected response to the quenching and partitioning would be the partial transformation of each austenite grain into martensite, followed by the enrichment of the balance untransformed austenite with carbon. The final microstructure, shown in Figure 14a, would then be a mixture of intercritical ferrite and martensitic islands interspersed with carbon-enriched retained austenite in martensite.

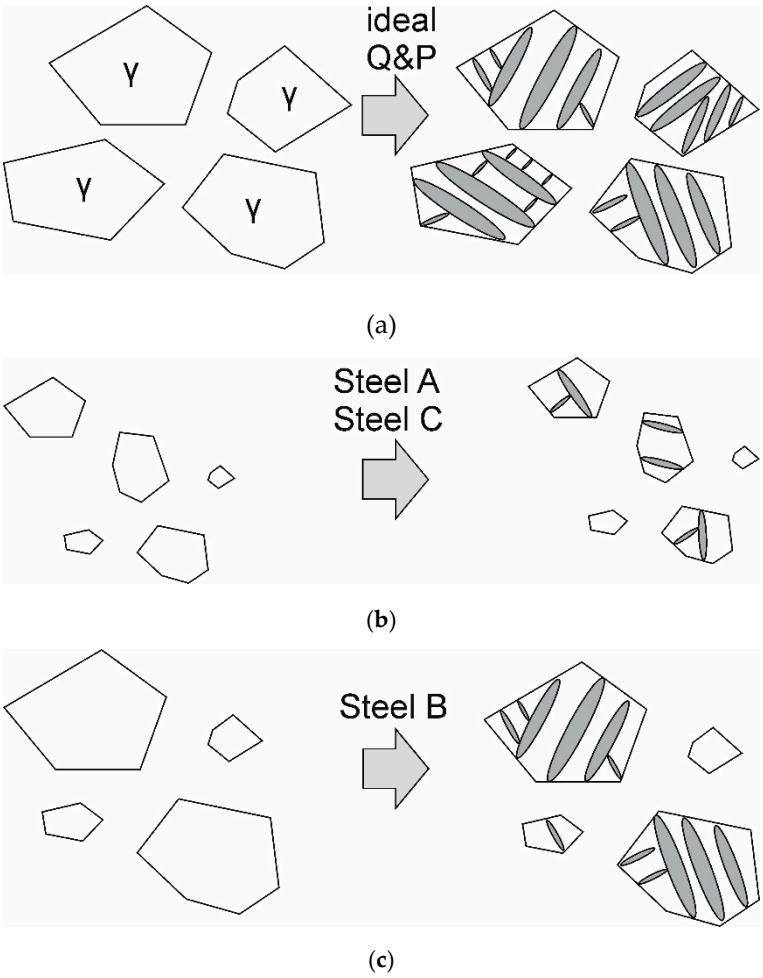

Figure 14. Austenite grains in a ferritic matrix partially transformed into martensite for (**a**) an ideal quenching and partitioning (Q&P) scenario, (**b**) the observed behavior of Steel A and Steel C and (**c**) the observed behavior of Steel B.

This type of microstructure was not observed in any of the studied grades. Instead, a complex microstructure had emerged in all cases consisting of intercritical ferrite, untransformed austenite grains and prior austenite grains in which the martensitic transformation had progressed to some degree.

This behavior can be attributed to two factors—the local chemical composition and the size of each austenite grain. During intercritical annealing, austenite will form at low-energy sites that are favorable towards nucleation [10]. In practice, this means ferrite grain boundaries and grain corners where the dissolution of cementite or other carbides has formed a carbon-rich volume suitable for nucleation. The stage of the annealing cycle at which each austenite grain nucleates will be decided by these local conditions. The growth rate of a nucleated austenite grain will, in turn, initially depend on the carbon content of the nucleus and at later stages the diffusion barrier formed by ferrite-stabilizing elements. In the case of the studied experimental steels, the primary element limiting austenite growth is aluminum, which is a strong ferrite stabilizer. As the austenite growth front advances, more and more aluminum will diffuse across the advancing front, until the aluminum content is high enough in the interfacial ferrite neighborhood and the growth slows down significantly.

The behavior during intercritical annealing can thus be characterized by a slow and uneven growth of austenite. Just prior to cooling, a microstructure has formed where exists a range of austenite grains with different sizes and chemical compositions. Such intercritical austenite microstructures are outlined schematically in Figure 14b,c.

Steel A and Steel C exhibited microstructures and mechanical properties quite similar and will be discussed together. Both steels have a similar chemical composition, with the notable differences being an elevated manganese content and a lower aluminum content in Steel A. This difference, along with the lower aluminum content, resulted in a slightly elevated austenite volume fraction after intercritical annealing in Steel A. In any case, both steels exhibit the type of intercritical austenite structure shown in Figure 14b, in which there are both very small and slightly larger austenite grains in the microstructure after annealing. When the steel in this condition is quenched to the quench temperature *QT*, primarily the larger, less stable austenite grains undergo a martensitic transformation, while the smaller, more stable grains remain unchanged. The less stable retained austenite is then stabilized with carbon during the partitioning stage. The result is a microstructure where the large, less stable austenite grains have become more refined and chemically stable due to martensitic transformation and subsequent rejection of supersaturated carbon during partitioning. Although only the larger austenite grains exhibit the expected quenched and partitioned response, the final result is a more homogenous, refined microstructure in terms of austenite stability, leading to the observed improvement in uniform elongation. Similar results have also been previously observed for steels with higher aluminum contents [3].

The quenching and partitioning response of Steel B is mostly explained by a greater fraction of intercritical austenite, along with a large distribution of austenite grain sizes and a larger average grain size overall. For Steel B, it is likely that bainite or isothermal martensite formation has occurred during partitioning, indicated by the large, irregularly shaped laths in Figure 11b. Another factor supporting bainite formation during partitioning is the high volume fraction of intercritical austenite (approximately 65 vol %). At 65 vol % austenite, assuming full partitioning of carbon, the austenite carbon concentration would be approximately 0.17 wt %. Compared to the Steels studied here with lower intercritical austenite fractions and consequentially higher carbon concentrations, Steel B is more amenable towards bainite (or, keeping in mind the high aluminum content, carbide-free bainite) formation during partitioning.

When Steel B is quenched to a sufficiently high temperature (in this case, 300 °C), the situation is similar to that observed for Steel A and Steel C: the smaller grains are left almost fully austenitic, while the larger grains transform to a greater degree (either to martensite or to carbide-free bainite). However, in this case, the smaller grains are left more unstable in the final microstructure; these unstable grains are transformed to martensite during the early stages of deformation, becoming unable to promote ductility at later stages. The message of this result is that to increase ductility, the end goal of the heat treatment should not be a perfect quenching and partitioning response, but the presence of highly stable retained austenite that will transform at a controlled stage of deformation. For Steels A and C, the quenching and partitioning treatment can be successfully used to refine and stabilize blocky-type austenite and increase the ductility of the steel, while at the same time introducing martensite into the microstructure. For Steel B, this is also possible to some degree, even though the tendency to form bainite or isothermal martensite during partitioning affects the final austenite fraction.

5. Conclusions

The quenching and partitioning response of three aluminum-alloyed experimental steels following intercritical annealing were investigated in this study. The following conclusions can be drawn from these investigations:

1. It is possible to produce quenched and partitioned dual-phase microstructures with superior mechanical properties using alloy compositions that can be processed with the current level of technology.
2. Each austenite grain undergoes martensitic transformation to a different degree at the initial quench temperature *QT* according to its mechanical and chemical stability.
3. Sufficiently stable austenite grains may remain completely untransformed.

The successful quenching and partitioning response of an intercritically annealed steel seems to largely depend on the state of the austenite prior to quenching. A sufficient carbon content and a small austenite grain size give the steels robust behavior with regard to heat treatment, when looking at Steels A and C. The martensitic transformation of these alloys can be controlled by varying *QT*.

Author Contributions: Conceptualization, T.N., O.O., P.J. and P.P.; methodology, T.N.; software, A.S.; validation, T.N.; formal analysis, T.N., M.S. and P.P.; investigation, T.N.; resources, O.O. and P.J.; data curation, T.N.; writing—original draft preparation, T.N.; writing—review and editing, T.N., P.P. and M.S.; visualization, T.N.; supervision, P.P.; project administration, T.N.; funding acquisition, P.P.

Funding: This research received no external funding.

Conflicts of Interest: The authors declare no conflict of interest.

References

1. Garcia, C.I.; Deardo, A.J. Formation of austenite in 1.5 pct Mn steels. *Metall. Trans. A* **1981**, *12*, 521–530. [CrossRef]
2. Speer, J.G.; Streicher, A.M.; Matlock, D.K.; Rizzo, F.C.; Krauss, G. Quenching and partitioning: A fundamentally new process to create high strength TRIP sheet microstructures. In Proceedings of the Symposium on the Thermodynamics, Kinetics, Characterization and Modeling of: Austenite Formation and Decomposition, Chicago, IL, USA, 9–12 November 2003; pp. 505–522.
3. Nyyssönen, T.; Peura, P.; De Moor, E.; Williamson, D.; Kuokkala, V.-T. Crystallography and mechanical properties of intercritically annealed quench and partitioned high-aluminum steel. *Mater. Charact.* **2019**, *148*, 71–80. [CrossRef]
4. Tan, X.; Ponge, D.; Lu, W.; Xu, Y.; Yang, X.; Rao, X.; Wu, D.; Raabe, D. Carbon and strain partitioning in a quenched and partitioned steel containing ferrite. *Acta Mater.* **2019**, *165*, 561–576. [CrossRef]
5. De Meyer, M.; Vanderschueren, D.; De Cooman, B.C. The Influence of the Substitution of Si by Al on the Properties of Cold Rolled C-Mn-Si TRIP Steels. *ISIJ Int.* **1999**, *39*, 813–822. [CrossRef]
6. Jacques, P.; Girault, E.; Catlin, T.; Geerlofs, N.; Kop, T.; van der Zwaag, S.; Delannay, F. Bainite transformation of low carbon Mn–Si TRIP-assisted multiphase steels: influence of silicon content on cementite precipitation and austenite retention. *Mater. Sci. Eng. A* **1999**, *273–275*, 475–479. [CrossRef]
7. Pierce, D.T.; Coughlin, D.R.; Clarke, K.D.; De Moor, E.; Poplawsky, J.; Williamson, D.L.; Mazumder, B.; Speer, J.G.; Hood, A.; Clarke, A.J. Microstructural evolution during quenching and partitioning of 0.2C-1.5Mn-1.3Si steels with Cr or Ni additions. *Acta Mater.* **2018**, *151*, 454–469. [CrossRef]
8. Nyyssönen, T.; Peura, P.; Kuokkala, V.-T. Crystallography, Morphology, and Martensite Transformation of Prior Austenite in Intercritically Annealed High-Aluminum Steel. *Metall. Mater. Trans. A* **2018**, *49*, 6426–6441. [CrossRef]
9. Datta, D.P.; Gokhale, A.M. Austenitization kinetics of pearlite and ferrite aggregates in a low carbon steel containing 0.15 wt pct C. *Metall. Trans. A* **1981**, *12*, 443–450. [CrossRef]
10. Shtansky, D.V.; Nakai, K.; Ohmori, Y. Pearlite to austenite transformation in an Fe–2.6Cr–1C alloy. *Acta Mater.* **1999**, *47*, 2619–2632. [CrossRef]
11. Nouri, A.; Saghafian, H.; Kheirandish, S. Effects of Silicon Content and Intercritical Annealing on Manganese Partitioning in Dual Phase Steels. *J. Iron Steel Res. Int.* **2010**, *17*, 44–50. [CrossRef]
12. Garcia, C.I.; Cho, K.; Redkin, K.; Deardo, A.J.; Tan, S.; Somani, M.; Karjalainen, L.P. Influence of Critical Carbide Dissolution Temperature during Intercritical Annealing on Hardenability of Austenite and Mechanical Properties of DP-980 Steels. *ISIJ Int.* **2011**, *51*, 969–974. [CrossRef]
13. Saunders, N.; Guo, U.K.Z.; Li, X.; Miodownik, A.P.; Schillé, J.-P. Using JMatPro to model materials properties and behavior. *JOM* **2003**, *55*, 60–65. [CrossRef]
14. Kirkaldy, J.; Doane, D. *Hardenability concepts with applications to steel*; Metallurgical society of AIME: New York, NY, USA, 1978.
15. Lee, J.-L.; Bhadeshia, H.K.D.H. A methodology for the prediction of time-temperature-transformation diagrams. *Mater. Sci. Eng. A* **1993**, *171*, 223–230. [CrossRef]
16. Yang, H.; Bhadeshia, H. Austenite grain size and the martensite-start temperature. *Scr. Mater.* **2009**, *60*, 493–495. [CrossRef]

17. Dong-Woo, S.; Kim, N.J.; Yi, H.L.; Chen, P.; Hou, Z.Y.; Hong, N.; Cai, H.L.; Xu, Y.B.; Wu, D.; Wang, G.D. A novel design: Partitioning achieved by quenching and tempering (Q–T & P) in an aluminium-added low-density steel. *Scr. Mater.* **2013**, *68*, 370–374.
18. Wang, X.; Liu, L.; Liu, R.D.; Huang, M.X. Benefits of Intercritical Annealing in Quenching and Partitioning Steel. *Metall. Mater. Trans. A* **2018**, *49*, 1460–1464. [CrossRef]
19. Maki, J.; Mahieu, J.; De Cooman, B.C.; Claessens, S. Galvanisability of silicon free CMnAl TRIP steels. *Mater. Sci. Technol.* **2003**, *19*, 125–131. [CrossRef]
20. Koistinen, D.P.; Marburger, R.E. A general equation prescribing the extent of the austenite-martensite transformation in pure iron-carbon alloys and plain carbon steels. *Acta Metall.* **1959**, *7*, 59–60. [CrossRef]
21. Vander Voort, G. *Metallography: Principles and Practice*; ASM International: Geauga County, OH, USA, 1984; ISBN 978-0-87170-672-0.
22. Jatczak, C.F.; Larsen, J.A.; Shin, S.W. *Retained Austenite and Its Measurements by X-Ray Diffraction; SP-453*; Society of Automotive Engineers, Inc.: Warrendale, PA, USA, 1980.
23. Cullity, B.D.; Stock, S.R. *Elements of X-Ray Diffraction*; Prentice Hall: Upper Saddle River, NJ, USA, 2001.
24. *ISO 2566-1:1984(E) Steel—Conversion of elongation values—Part 1: Carbon and low alloy steels*; International Organization for Standardization: Vernier, Switzerland, 1984; pp. 1–28.
25. Bhadeshia, H.K.D.H. Thermodynamic extrapolation and martensite-start temperature of substitutionally alloyed steels. *Met. Sci.* **1981**, *15*, 178–180. [CrossRef]
26. Bhadeshia, H.K.D.H. Driving force for martensitic transformation in steels. *Met. Sci.* **1981**, *15*, 175–177. [CrossRef]
27. Nyyssönen, T.; Isakov, M.; Peura, P.; Kuokkala, V.-T. Iterative Determination of the Orientation Relationship between Austenite and Martensite from a Large Amount of Grain Pair Misorientations. *Metall. Mater. Trans. A* **2016**, *47*, 2587–2590. [CrossRef]
28. Bhadeshia, H.K.D.H. An aspect of the nucleation of burst martensite. *J. Mater. Sci.* **1982**, *17*, 383–386. [CrossRef]

© 2019 by the authors. Licensee MDPI, Basel, Switzerland. This article is an open access article distributed under the terms and conditions of the Creative Commons Attribution (CC BY) license (http://creativecommons.org/licenses/by/4.0/).